Article

Ruthenium Porphyrin Functionalized Single-Walled Carbon Nanotube Arrays#A Step Toward Light Harvesting Antenna and Multibit Information Storage

Jingxian Yu, Simon Mathew, Benjamin S. Flavel, Martin R. Johnston, and Joe G. Shapter

J. Am. Chem. Soc., **2008**, 130 (27), 8788-8796 • DOI: 10.1021/ja801142k • Publication Date (Web): 14 June 2008

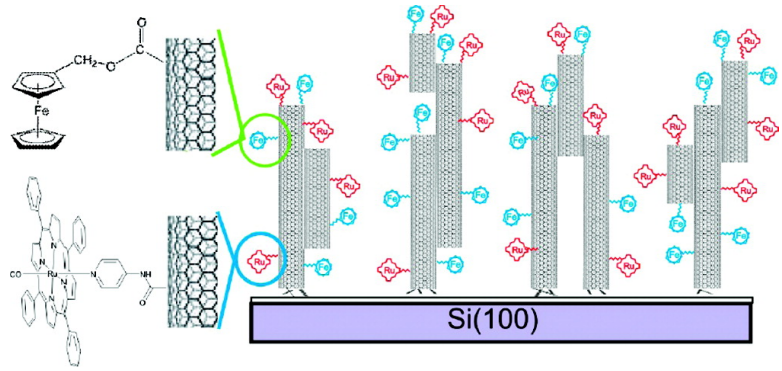

J|A|C|S
ARTICLES

Published on Web 06/14/2008

Ruthenium Porphyrin Functionalized Single-Walled Carbon Nanotube Arrays—A Step Toward Light Harvesting Antenna and Multibit Information Storage

Jingxian Yu, Simon Mathew, Benjamin S. Flavel, Martin R. Johnston, and Joe G. Shapter*

School of Chemistry, Physics and Earth Sciences, Flinders University, Bedford Park, SA 5042, Australia

Received March 2, 2008; E-mail: Joe.shapter@flinders.edu.au

Abstract: Ruthenium porphyrin functionalized single-walled carbon nanotube arrays have been prepared using coordination of the axial position of the metal ion onto 4-aminopyridine preassembled single-walled carbon nanotubes directly anchored to a silicon(100) surface (SWCNTs-Si). The formation of these ruthenium porphyrin functionalized single-walled carbon nanotube array electrodes (RuTPP-SWCNTs-Si) has been monitored using infrared spectroscopy (IR), differential pulse voltammetry (DPV), atomic force microscopy (AFM), laser desorption time-of-flight mass spectroscopy (LDI-TOF-MS), UV−vis spectroscopy, fluorescence spectroscopy, and cyclic voltammetry. Electrochemical results show two successive one-electron reversible redox waves. The surface concentration of the ruthenium porphyrin molecules is 3.44×10^{-8} mol cm^{-2}. Optical results indicate that the immobilization of ruthenium porphyrin enhances the light absorption of SWCNTs-Si surfaces in the visible light region. Moreover mixed assembly of ferrocene/porphyrin onto carbon nanotube arrays has been achieved by altering the ratio of two redox-active species in the deposition solution. These results suggest the ruthenium porphyrin modified electrodes are excellent candidates for molecular memory devices and light harvesting antennae.

Introduction

Single-walled carbon nanotubes (SWCNTs) have recently become the focus of intense multidisciplinary study due to their unique structure, chirality-dependent conductivity, high mechanical strength, and good chemical stability.[1,2] Various potential applications, including those in chemical and biochemical sensors[3–5] as well as nanoelectronic and optoelectronic devices,[6–11] have been widely explored. However, most of these potential applications require the chemical modification of carbon nanotubes with specific functionalities.[12] So far, a wide range of electrochemical active species, biological molecules, and nanoparticles, including DNA,[5,13,14] proteins,[15–18] ferrocene,[17,19,20] porphyrins,[21,22] and CdS nanoparticles[23] have been exploited.

Because porphyrins are stable natural functional dyes with a large extinction coefficient in the visible light region, have predictable rigid structures, and possess prospective photochemical electron-transfer ability,[24] they are often used as visible chromophores to decorate the surface of semiconductor and

(1) Iijima, S.; Ichihashi, T. *Nature* **1993**, *363*, 603–605.
(2) Bethune, D. S.; Kiang, C. H.; Devries, M. S.; Gorman, G.; Savoy, R.; Vazquez, J.; Beyers, R. *Nature* **1993**, *363*, 605–607.
(3) Kong, J.; Franklin, N. R.; Zhou, C. W.; Chapline, M. G.; Peng, S.; Cho, K. J.; Dai, H. J. *Science* **2000**, *287*, 622–625.
(4) Collins, P. G.; Bradley, K.; Ishigami, M.; Zettl, A. *Science* **2000**, *287*, 1801–1804.
(5) Jung, D. H.; Kim, B. H.; Ko, Y. K.; Jung, M. S.; Jung, S.; Lee, S. Y.; Jung, H. T. *Langmuir* **2004**, *20*, 8886–8891.
(6) Tans, S. J.; Devoret, M. H.; Dai, H. J.; Thess, A.; Smalley, R. E.; Geerligs, L. J.; Dekker, C. *Nature* **1997**, *386*, 474–477.
(7) Bockrath, M.; Cobden, D. H.; McEuen, P. L.; Chopra, N. G.; Zettl, A.; Thess, A.; Smalley, R. E. *Science* **1997**, *275*, 1922–1925.
(8) Tans, S. J.; Verschueren, A. R. M.; Dekker, C. *Nature* **1998**, *393*, 49–52.
(9) Collins, P. G.; Zettl, A.; Bando, H.; Thess, A.; Smalley, R. E. *Science* **1997**, *278*, 100–103.
(10) Fuhrer, M. S.; Nygard, J.; Shih, L.; Forero, M.; Yoon, Y. G.; Mazzoni, M. S. C.; Choi, H. J.; Ihm, J.; Louie, S. G.; Zettl, A.; McEuen, P. L. *Science* **2000**, *288*, 494–497.
(11) Liu, X. L.; Han, S.; Zhou, C. W. *Nano Lett.* **2006**, *6*, 34–39.
(12) Li, H. P.; Martin, R. B.; Harruff, B. A.; Carino, R. A.; Allard, L. F.; Sun, Y. P. *Adv. Mater.* **2004**, *16*, 896–900.
(13) He, P. G.; Dai, L. M. *Chem. Commun.* **2004**, 348–349.
(14) Gooding, J. J.; Mearns, F.; Yang, W. R.; Liu, J. Q. *Electroanalysis* **2003**, *15*, 81–96.
(15) Liu, J. Q.; Chou, A.; Rahmat, W.; Paddon-Row, M. N.; Gooding, J. J. *Electroanalysis* **2005**, *17*, 38–46.
(16) Gooding, J. J.; Wibowo, R.; Liu, J. Q.; Yang, W. R.; Losic, D.; Orbons, S.; Mearns, F. J.; Shapter, J. G.; Hibbert, D. B. *J. Am. Chem. Soc.* **2003**, *125*, 9006–9007.
(17) Liu, J. Q.; Paddon-Row, M. N.; Gooding, J. J. *J. Phys. Chem. B* **2004**, *108*, 8460–8466.
(18) Patolsky, F.; Weizmann, Y.; Willner, I. *Angew. Chem., Int. Ed.* **2004**, *43*, 2113–2117.
(19) Yu, J.; Shapter, J. G.; Johnston, M. R.; Quinton, J. S. *Electrochim. Acta* **2007**, *52*, 6206–6211.
(20) Guldi, D. M.; Marcaccio, M.; Paolucci, D.; Paolucci, F.; Tagmatarchis, N.; Tasis, D.; Vazquez, E.; Prato, M. *Angew. Chem., Int. Ed.* **2003**, *42*, 4206–4209.
(21) Ren, D. M.; Guo, Z.; Du, F.; Zheng, J. Y.; Chen, Y. S. *J. Nanosci. Nanotechno.* **2007**, *7*, 1539–1545.
(22) Salimi, A.; MamKhezri, H.; Hallaj, R.; Zandi, S. *Electrochim. Acta* **2007**, *52*, 6097–6105.
(23) Sheeney-Haj-Khia, L.; Basnar, B.; Willner, I. *Angew. Chem., Int. Ed.* **2005**, *44*, 78–83.
(24) Guo, Z.; Du, F.; Ren, D. M.; Chen, Y. S.; Zheng, J. Y.; Liu, Z. B.; Tian, J. G. *J. Mater. Chem.* **2006**, *16*, 3021–3030.

10.1021/ja801142k CCC: $40.75

metal nanoparticles.[25,26] However an important issue in these systems is the quenching of the dye's photoexcited states by nanoparticles, which results in a low quantum yield for the desired charge separation.[27,28] Carbon nanotubes are being considered as an alternative to nanoparticles in photovoltaic devices.[23,29,30] Incorporation of light absorbing antenna chromophores, such as porphyrins, through a covalent linkage with the extended π electrons of a carbon nanotube would constitute an ideal supramolecular nanoassembly for generating singlet excited energy and its conversion to chemical energy.[12,31] Baskaran and his co-workers[31] synthesized and characterized MWCNTs and SWCNTs with covalently linked porphyrin antennae as potential supramolecular donor−acceptor complexes. The absorption and fluorescence of these complexes showed that the carbon nanotubes serve as an efficient electron acceptor and pave the way to construct novel photovoltaic devices and light-harvesting systems using various porphyrin-functionalized carbon nanotubes. Kamat and his co-workers[32] constructed photochemical solar cells from organized assemblies of single-walled carbon nanotubes (SWCNTs) and protonated porphyrin on nanostructured SnO_2 electrodes and observed the dual role of SWCNTs in promoting photoinduced charge separation and facilitating charge transport.

Simultaneously porphyrins have also been attracting much attention as information storage media because they exhibit a number of key properties:[33–35] (1) they form π-cation radicals that are relatively stable under ambient conditions, (2) they exhibit multiple cationic states that afford multibit information storage and (3) they are capable of storing charge for extended periods, up to tens of minutes, significantly attenuating the refresh rates required in a memory device. Bocian and his co-workers[34] demonstrated that porphyrin-based molecules bound to Si(100) exhibit redox behavior useful for information storage. These molecular media in an inert atmosphere are stable under extremes of temperature (400 °C) for extended periods (approaching 1 h) and do not degrade under large numbers of read−write cycles (10^{12}).

Recently Garcia and co-workers[36] have reported the interaction of zinc porphyrin with pyridyl functionalized SWCNTs through an apical coordinative bond between the porphyrin transition metal atom and the pyridyl ligand. We have demonstrated surface-mounted ferrocene using covalent immobilization of an alcohol substituted ferrocene derivative to preassembled single-walled carbon nanotubes directly anchored to silicon(100) surface (SWCNTs-Si).[19]In this paper, we will present the preparation and characterization of ruthenium porphyrin modified carbon nanotube arrays and demonstrate their potential applications for information storage and light harvesting antennae.

Experimental Section

Preparation of Ruthenium Porphyrin Modified SWCNT Arrays Covalently Anchored to Silicon(100) (RuTPP-SWCNTs-Si). Highly boron doped p-type silicon(100) wafers (0.5 mm thickness, 1 mΩ·cm resistance, and polished on one side) were purchased from Virginia Semiconductor, Inc., USA. The preparation of vertically aligned shortened carbon nanotube architectures on a silicon(100) substrate (SWCNTs-Si) by chemical anchoring directly to the surface followed the procedure reported in our earlier work.[19,37] The schematic representation of the preparation of ruthenium porphyrin RuTPP(CO)(EtOH) coordinated to single-walled carbon nanotube arrays directly attached to a p-type silicon(100) surface (RuTPP-SWCNTs-Si) is schematically summarized in Figure 1. After the SWCNTs-Si structures were rinsed with a copious amount of acetone (99.5%, Merck) to remove any unbound reagents and dried with high purity nitrogen flow, they were incubated in a *N,N'*-dimethylformamide (DMF, 99.8%, Aldrich) solution containing 0.01 mol L^{-1} 4-aminopyridine (≥99%, Aldrich), 0.5 mg mL^{-1} 1,3-dicyclohexylcarbodiimide (DCC, 99%, Aldrich) and 0.05 mg mL^{-1} 4-(dimethylamino) pyridine (DMAP) for 24 h at room temperature. The role of DCC is critical in facilitating the ester and amide coupling reactions used in the synthesis of the target surface by enabling the mounting of functionalized SWCNTs and 4-aminopyridine, respectively, through the production of activated ester intermediates.[38] The role of DMAP is as a nucleophilic catalyst in the esterification reaction of functionalized SWCNTs to the hydroxylated Si surface. The use of DMAP is also critical in the subsequent amidation reaction between 4-aminopyridine and the remaining carboxylic acid residues on the nanotubes on the SWCNTs-Si surface.[39–41] The 4-aminopyridine mounted SWCNTs-Si surfaces were rinsed with DMF and chloroform (Merck. Germany) in turn to remove any physically absorbed chemicals and then immersed in a 0.5 mg mL^{-1} ruthenium porphyrin/chloroform solution for 24 h. The resulting surfaces were washed with a copious amount of chloroform and then stored in the dark after being dried by a high purity nitrogen stream.

Preparation of Mixed Ferrocenemethanol and Ruthenium Porphyrin Modified SWCNTs-Si (Fc/RuTPP-SWCNTs-Si). SWCNTs-Si architectures were immersed in DMF solutions containing 0.5 mg mL^{-1} DCC, 0.05 mg mL^{-1} 4-(dimethylamino)pyridine, and different molar ratios of 4-aminopyridine and ferrocenemethanol (97%, Aldrich) for 24 h, where the concentration of 4-aminopyrdine was kept constant at 0.01 mol L^{-1}. The process gave ferrocenemethanol and 4-aminopyridine covalently bound mixed assembled SWCNTs-Si. The resulting surfaces were subsequently washed with DMF and chloroform solvents to remove any unreacted reagents, then immersed in a chloroform solution of

(25) Kanayama, N.; Kanbara, T.; Kitano, H. *J. Phys. Chem. B* **2000**, *104*, 271–278.
(26) Lahav, M.; Heleg-Shabtai, V.; Wasserman, J.; Katz, E.; Willner, I.; Durr, H.; Hu, Y. Z.; Bossmann, S. H. *J. Am. Chem. Soc.* **2000**, *122*, 11480–11487.
(27) Imahori, H.; Yamada, H.; Guldi, D. M.; Endo, Y.; Shimomura, A.; Kundu, S.; Yamada, K.; Okada, T.; Sakata, Y.; Fukuzumi, S. *Angew. Chem., Int. Ed.* **2002**, *41*, 2344–2347.
(28) Yamada, H.; Imahori, H.; Nishimura, Y.; Yamazaki, I.; Ahn, T. K.; Kim, S. K.; Kim, D.; Fukuzumi, S. *J. Am. Chem. Soc.* **2003**, *125*, 9129–9139.
(29) Satake, A.; Miyajima, Y.; Kobuke, Y. *Chem. Mater.* **2005**, *17*, 716–724.
(30) Campidelli, S.; Sooambar, C.; Diz, E. L.; Ehli, C.; Guldi, D. M.; Prato, M. *J. Am. Chem. Soc.* **2006**, *128*, 12544–12552.
(31) Baskaran, D.; Mays, J. W.; Zhang, X. P.; Bratcher, M. S. *J. Am. Chem. Soc.* **2005**, *127*, 6916–6917.
(32) Hasobe, T.; Fukuzumi, S.; Kamat, P. V. *J. Phys. Chem. B* **2006**, *110*, 25477–25484.
(33) Roth, K. M.; Yasseri, A. A.; Liu, Z. M.; Dabke, R. B.; Malinovskii, V.; Schweikart, K. H.; Yu, L. H.; Tiznado, H.; Zaera, F.; Lindsey, J. S.; Kuhr, W. G.; Bocian, D. F. *J. Am. Chem. Soc.* **2003**, *125*, 505–517.
(34) Liu, Z. M.; Yasseri, A. A.; Lindsey, J. S.; Bocian, D. F. *Science* **2003**, *302*, 1543–1545.
(35) Li, Q. L.; Surthi, S.; Mathur, G.; Gowda, S.; Zhao, Q.; Sorenson, T. A.; Tenent, R. C.; Muthukumaran, K.; Lindsey, J. S.; Misra, V. *Appl. Phys. Lett.* **2004**, *85*, 1829–1831.
(36) Alvaro, M.; Atienzar, P.; la Cruz, P.; Delgado, J. L.; Troiani, V.; Garcia, H.; Langa, F.; Palkar, A.; Echegoyen, L. *J. Am. Chem. Soc.* **2006**, *128*, 6626–6635.
(37) Yu, J. X.; Shapter, J. G.; Quinton, J. S.; Johnston, M. R.; Beattie, D. A. *PCCP* **2007**, *9*, 510–520.
(38) Khorana, H. G. *Chem. Rev.* **1953**, *53*, 145.
(39) Berry, D. J.; Digiovanna, C. V.; Metrick, S. S.; Murugan, R. *Arkivoc* **2001**, *2*, 944–964.
(40) Höfle, G.; Steglich, W.; Vorbrüggen, H. *Angew. Chem., Int. Ed.* **1978**, *17*, 569–583.
(41) Xu, S. J.; Held, I.; Kempf, B.; Mayr, H.; Steglich, W.; Zipse, H. *Chem.—Eur. J.* **2005**, *11*, 4751–4757.

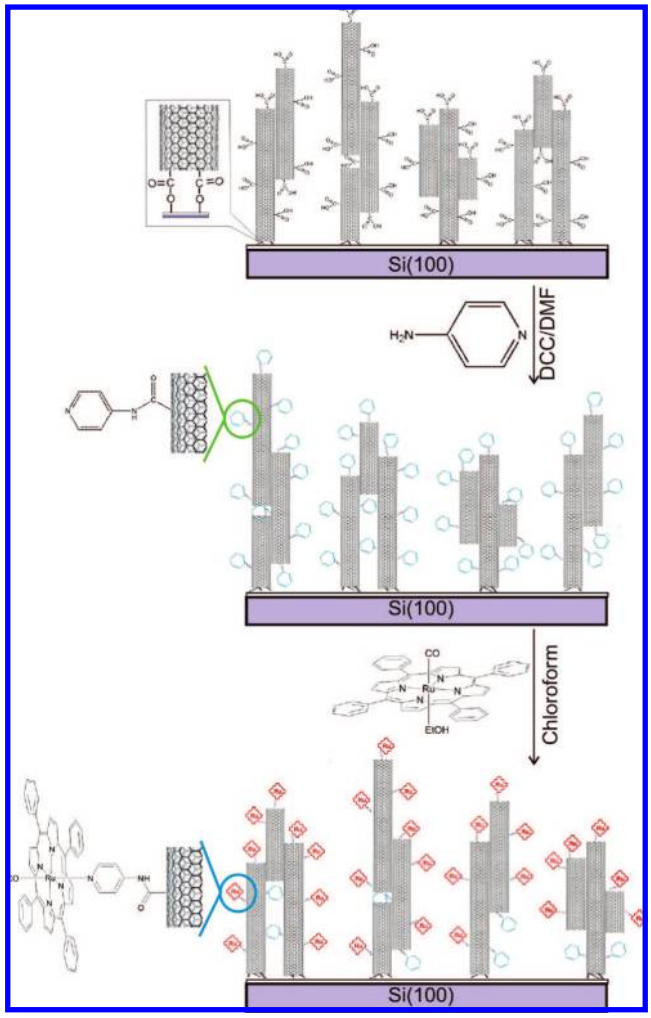

Figure 1. Schematic representation of the preparation of ruthenium porphyrin (RuTPP) coordinated to single-walled carbon nanotube (SWCNT) array directly attached to a p-type silicon(100) (RuTPP-SWCNTs-Si).

0.5 mg mL^{-1} ruthenium porphyrin RuTPP(CO)(EtOH) for 24 h. The metalloporphyrin coordinated to the surface-mounted 4-aminopyridine forming a mixed assembly of ferrocenemethanol and ruthenium porphyrin on the SWCNTs-Si surface (Fc/RuTPP-SWCNTs-Si).

Infrared Spectroscopy. The FTIR spectra of 4-aminopyridine and ruthenium porphyrin modified SWCNTs-Si were acquired by placing silicon(100) plates carefully with the polished side of the wafer facing down and contacting with a flat ZnSe ATR crystal (50 mm × 10 mm × 3 mm size, 45° bevel angle). The analysis angle was set to 45° for the variable angle horizontal ATR accessory (Pike Technologies, Inc., USA). A silicon(100) wafer with a native oxide layer was used as the reference spectrum. The FTIR spectra of solid phase 4-aminopyridine and ruthenium porphyrin were obtained by dropping their chloroform solutions onto the ATR crystal and forming an evenly covered solid phase layer. FTIR spectra were measured using a Bio-RAD FTS-40A spectrometer equipped with an MCT (mercury cadmium telluride) detector cooled with liquid nitrogen. All of the spectra were recorded by integrating 256 interferograms in the wavenumber range (1000−4000 cm^{-1}) with a resolution of 2 cm^{-1}. The ZnSe crystal was cleaned with neat tetrahydrofuran before every experiment, and the ATR accessory was purged with dry N_2 during data acquisition.

Atomic Force Microscopy (AFM). Atomic Force Microscope tapping mode images were taken in air with a multimode head and Nanoscope IV controller (Digital Instruments, Veeco, Santa Barbara). Commercially available silicon cantilevers (FESP-ESP series, Veeco probes, Santa Barbara) with the fundamental resonance frequency between 70−85 kHz were used. Topographic (height) and amplitude images were obtained simultaneously at a scan rate of 1 Hz with the parameters of set point, amplitude, scan size, and feedback control optimized for each sample. All images presented represent background subtracted data using the "flatten" feature in the Digital Instruments software.

Mass Spectroscopy. Laser-Desorption Time-of-Flight Mass Spectrometry (LDI-TOF-MS) spectra were acquired using a Micromass M@LDI instrument (Waters, UK) with a 337 nm pulsed N_2 laser. The instrument was operated in positive ion reflection mode with pulse voltage 2500 V and reflection voltage 2000 V.

Solid State UV−vis Spectroscopy. UV−vis spectra were measured using a Cary 5G UV−vis−NIR spectrophotometer equipped with an Absphere biconical accessory. All of the spectra were recorded by averaging 25 scans in the wavenumber range 400−600 cm^{-1} with a scan rate of 10 nm min^{-1}. A silicon(100) substrate with a native oxide layer was used as the reference sample.

Fluorescence Spectroscopy. A Cary Eclipse Fluorescence spectrometer equipped with solid sample holder accessory was used to investigate the fluorescence properties of SWCNTs-Si, 4-aminopyridine mounted SWCNTs-Si and RuTPP-SWCNTs-Si surfaces. Hydroxyl terminated silicon (100) was used as a reference surface. The fluorescence emission spectra were obtained with both excitation and emission slit widths of 20 nm.

Electrochemical Measurements. All electrochemical experiments were carried out in a specially designed electrochemical cell described previously.[37] The RuTPP-SWCNTs-Si and Fc/RuTPP-SWCNTs-Si surfaces were used as working electrodes. A polypropylene pipet (∼1 mL) tip, containing a platinum wire counter electrode, a bare silver wire (Ag^+/Ag) reference electrode and electrolyte solution, was pressed down against the silicon samples. Since tetra-n-butylammonium hexafluorophosphate ($TBAPF_6$) as supporting electrolyte could give a greater separation between the first and second oxidation peaks for porphyrins than tetra butylammomium perchlorate (TBAP),[42,43] 0.1 mol L^{-1} $TBAPF_6$ (≥99%, Fluka)/CH_2Cl_2 (Isocratic HPLC grade, Scharlau Chemie) solution was used as the electrolyte. All electrochemical experiments were performed inside a drybox filled with high purity N_2 using a BAS 100B Electrochemical Analyzer at room temperature.

Results and Discussion

Infrared Spectroscopy of RuTPP-SWCNTs-Si Structure. The 4-aminopyridine mounted single-walled carbon nanotube arrays were initially examined by FTIR. The FTIR spectrum of solid phase 4-aminopyridine is shown in Figure 2a, which is similar to the IR spectrum reported by the Spectral Database for Organic Compounds.[44] Peaks can be observed at 3435, 3289, 3074, 1647, 1598, 1507, and 990 cm^{-1}. The peaks at 3435 and 3289 cm^{-1} are attributed to the N−H stretching.[45,46] The C−H stretching vibrations are usually observed in the range 3000−3100 cm^{-1}.[47] Ring stretching vibrations occur in the general region 1600−1300 cm^{-1}.[48]

These vibrations involve stretching and contraction of all the bonds in the ring and interaction between the stretching modes.

(42) Kadish, K. M.; Lin, M.; Van Caemelbecke, E.; De Stefano, G.; Medforth, C. J.; Nurco, D. J.; Nelson, N. Y.; Krattinger, B.; Muzzi, C. M.; Jaquinod, L.; Xu, Y.; Shyr, D. C.; Smith, K. M.; Shelnutt, J. A. *Inorg. Chem.* **2002**, *41*, 6673–6687.
(43) Bhyrappa, P.; Sankar, M.; Varghese, B. *Inorg. Chem.* **2006**, *45*, 4136–4149.
(44) In *http://riodb01.ibase.aist.go.jp/*; National Institute of Advanced Industrial Science and Technology (AIST), Japan.
(45) Wong, K. N.; Colson, S. D. *J. Mol. Spectrosc.* **1984**, *104*, 129–151.
(46) Kline, C. H.; Turkevich, J. *J. Chem. Phys.* **1944**, *12*, 300–309.
(47) Roeges, N. P. G. *A Guide to the Complete Interpretation of Infrared Spectra of Organic Structures*; Wiley: New York, 1994.
(48) Corrsin, L.; Fax, B. J.; Lord, R. C. *J. Chem. Phys.* **1953**, *21*, 1170–1176.

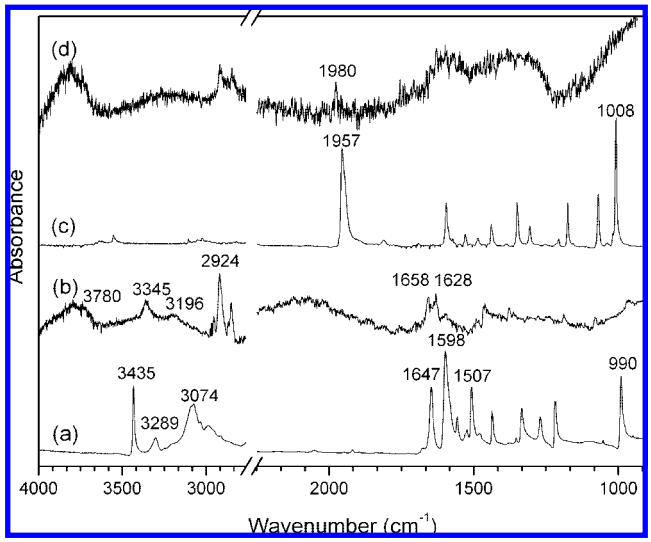

Figure 2. FTIR spectra of (a) solid phase 4-aminopyridine, (b) 4-aminopyridine mounted SWCNTs-Si surface, (c) solid phase ruthenium porphyrin (RuTPP(CO)(EtOH)), and (d) ruthenium porphyrin coordinated to 4-aminopyridine modified SWCNTs-Si.

The peak at 990 cm^{-1} is assigned to the pyridine ring breathing mode.[49] For 4-aminopyridine mounted single walled carbon nanotube arrays, the signal/noise ratio of FTIR spectrum (shown as curve b in Figure 2) becomes lower but absorption peaks at 3780, 3345, 2924, 1658 and 1628 cm^{-1} are still observed. By comparison with the IR spectra of solid phase 4-aminopyrdine and SWCNTs-Si structures,[37] the new doublet peaks at 1658 and 1628 cm^{-1} are attributed to carbonyl stretching of the pyridyl-nanotube amide, which proves that 4-aminopyridine molecules have been covalently immobilized onto the carbon nanotube array via the formation of amide groups. The peaks at 3345, 3196 and 2924 cm^{-1} originate from the peaks at 3435, 3289, 3074 cm^{-1} in Figure 2 (a), but shift to lower frequencies because of their covalent immobilization onto SWCNTs-Si surface. Since the broad and strong absorption peak observed at 3780 cm^{-1} has higher vibration frequency than OH stretching observed at SWCNTs-Si surface,[37] this absorption should be due to the N−H stretching from the newly formed pyridyl-nanotube amide groups.

Figure 2 (c) shows the FTIR spectrum of solid phase ruthenium porphyrin RuTPP(CO)(EtOH). Several strong absorption peaks can be observed including peaks at 1957 and 1008 cm^{-1}, which are attributed to carbonyl stretching[50,51] and the porphyrin pyrrole ring breathing mode, respectively.[52,53] After 4-aminopyridine mounted SWCNTs-Si surfaces were immersed in a chloroform solution of 0.5 mg mL^{-1} ruthenium porphyrin for 24 h, the FTIR spectrum shown in Figure 2d is observed. The absorption of the axial carbonyl ligand slightly shifted from 1957 cm^{-1} in the starting material to 1980 cm^{-1} when surface mounted. This shift to higher wavenumbers is consistent with axial coordination to the metal atom. Thus the

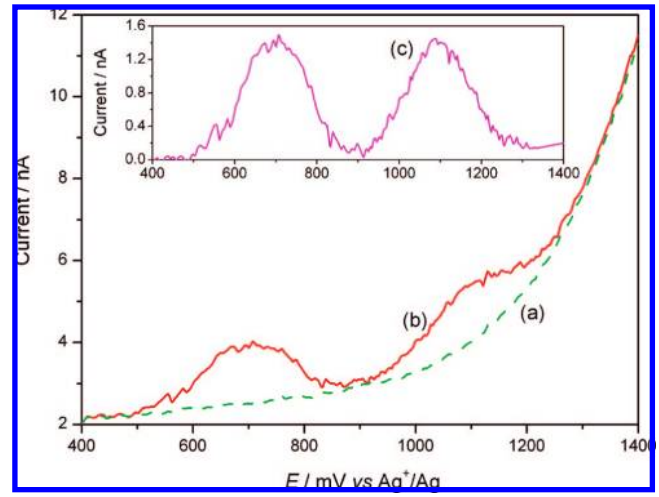

Figure 3. Differential pulse voltammograms of ruthenium porphyrin coordinated to 4-aminopyridine modified SWCNTs-Si surfaces in 0.1 mol L^{-1} $TBAPF_6/CH_2Cl_2$ solution at the scan rate 20 mV s^{-1} after SWCNTs-Si surfaces were immersed in 0.01 mol L^{-1} 4-aminopyridine/DMF (a) without and (b) with 0.5 mg mL^{-1} DCC and 0.05 mg mL^{-1} 4-(dimethylamino)pyridine for 24 h, and subsequently incubated in 0.5 mg mL^{-1} RuTPP(CO)(EtOH)/$CHCl_3$ solution for 24 h at room temperature. Curve (c) is the difference spectrum by subtracting curve (a) from curve (b).

IR analysis indicated that ruthenium porphyrin has self-assembled onto the carbon nanotube array by coordination of immobilized 4-aminopyridine moieties at the axial position of the metal ion.[51,54,55] The coverage of porphyrin appears to be very low. It is envisaged that the metalloporphyrin is blocking adjacent aminopyridyl moieties from complexation with other porphyrins. The steric bulk provided by the dye molecule appears to be denying aminopyridyl groups on the surface-mounted nanotubes access to the porphyrin solution, thereby inhibiting total complexation of the pyridyl residues by RuTPP.

Voltammetric Behavior. To confirm the coordination of ruthenium porphyrin onto 4-aminopyridine covalently immobilized SWCNTs-Si, differential pulse voltammograms (shown in Figure 3) were measured after SWCNTs-Si surfaces were exposed first to 4-aminopyridine and 4-(dimethylamino)pyridine (a) without and (b) with DCC followed by incubation in a RuTPP(CO)(EtOH) solution. From curve (a), no peaks can be observed after SWCNTs-Si surfaces were immersed without DCC and DMAP coupling agents. However two peaks at 751 and 1041 mV (vs Ag^+/Ag) can be observed when DCC and DMAP are included during the deposition procedure.

Due to the electron withdrawing effect of the electronegative nitrogen atom on the pyridine ring, the reactivity of the amine group becomes low. When SWCNTs-Si surfaces are immersed into 4-aminopyridine/DMF solution with DCC, carboxylic groups at the free ends of shortened SWCNTs will be converted to active carbodiimide esters.[16,56] The condensation reaction between the amine group in 4-aminopyridine and carboxylic groups in SWCNTs gets easier with DMAP and DCC present. Curve (c) shows the difference voltammogram obtained by subtracting curve (a) from curve (b), which exhibits two well separated oxidation peaks with very similar peak areas and with a peak separation of 290 mV. Similar results can be observed on the cyclic voltammograms of ruthenium porphyrin coordi-

(49) Panicker, C. Y.; Varghese, H. T.; Philip, D.; Nogueira, H. I. S. *Spectrochim. Acta A* **2006**, *64*, 744–747.
(50) Prodi, A.; Indelli, M. T.; Kleverlaan, C. J.; Scandola, F.; Alessio, E.; Gianferrara, T.; Marzilli, L. G. *Chem.—Eur. J.* **1999**, *5*, 2668–2679.
(51) Funatsu, K.; Kimura, A.; Imamura, T.; Ichimura, A.; Sasaki, Y. *Inorg. Chem.* **1997**, *36*, 1625–1635.
(52) Yasseri, A. A.; Syomin, D.; Loewe, R. S.; Lindsey, J. S.; Zaera, F.; Bocian, D. F. *J. Am. Chem. Soc.* **2004**, *126*, 15603–15612.
(53) Li, X. Y.; Czernuszewicz, R. S.; Kincaid, J. R.; Stein, P.; Spiro, T. G. *J. Phys. Chem.* **1990**, *94*, 47–61.
(54) Kimura, A.; Funatsu, K.; Imamura, T.; Kido, H.; Sasaki, Y. *Chem. Lett.* **1995**, 207–208.
(55) Kariya, N.; Imamura, T.; Sasaki, Y. *Inorg. Chem.* **1997**, *36*, 833–839.

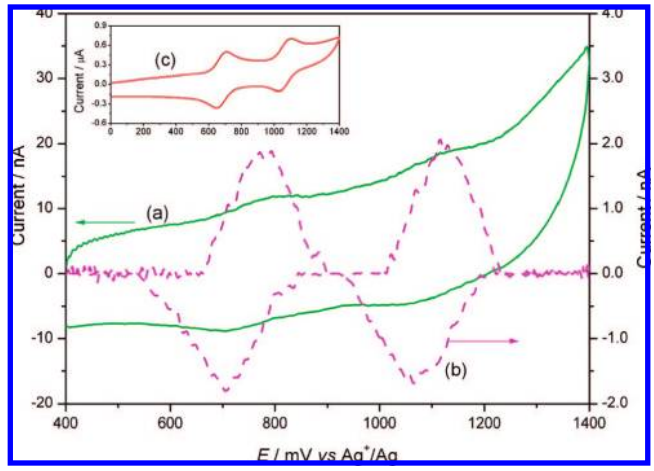

Figure 4. Cyclic voltammograms of ruthenium porphyrin coordinated to 4-aminopyridine modified SWCNTs-Si surfaces in 0.1 mol L^{-1} $TBAPF_6/CH_2Cl_2$ solution at the scan rate 20 mV s^{-1}. (a) The original CV curve and (b) the CV curve after baseline subtraction. Inset: Cyclic voltammogram of 1 mmol L^{-1} ruthenium porphyrin contained in 0.1 mol L^{-1} $TBAPF_6/CH_2Cl_2$ solution on a gold electrode.

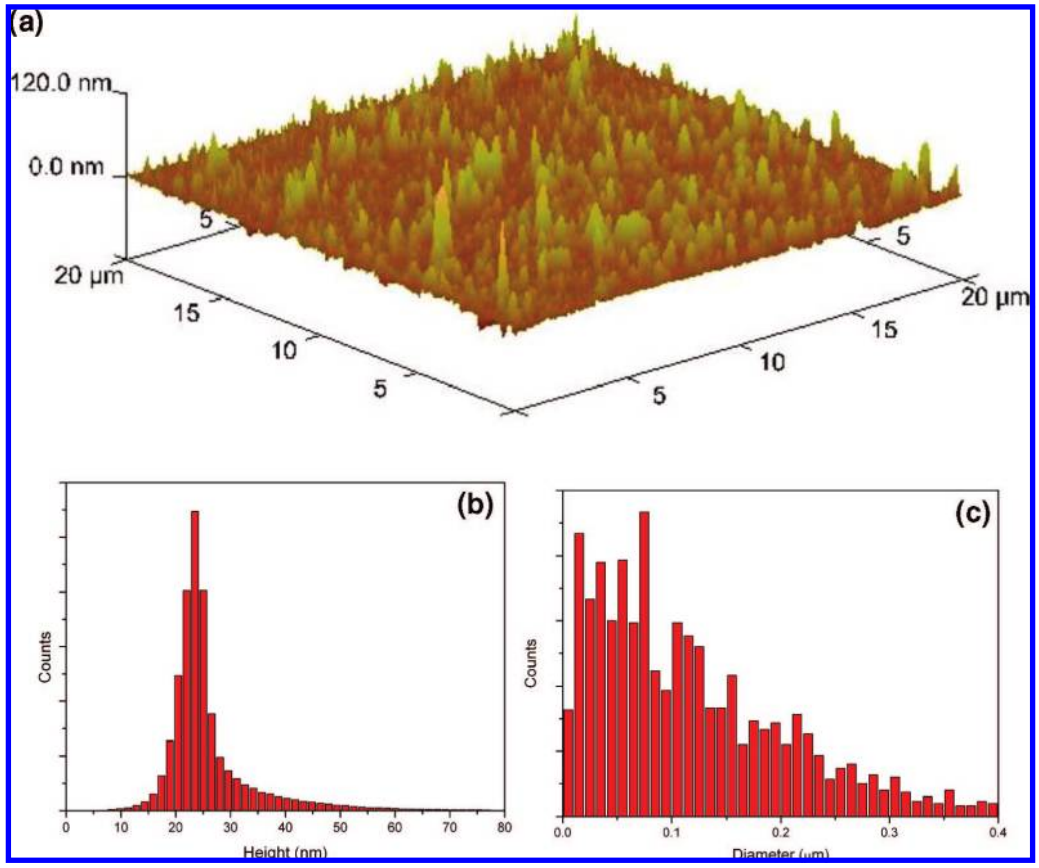

Figure 5. (a) Tapping mode AFM image of the RuTPP-SWCNTs-Si surface formed after 4-aminopyridine surface-mounted SWCNTs-Si surface was immersed in ruthenium porphyrin/$CHCl_3$ solution for 24 h at room temperature. (b) Height distribution of carbon nanotubes. (c) Width distribution of carbon nanotubes.

nated to 4-aminopyridine modified surfaces (shown in Figure 4). A significant background current and two pairs of redox peaks are observed. A large background current is expected because of the rough surface observed by AFM (shown in Figure 5) and due to pseudocapacitances related to surface Faradaic processes of redox active species.[57] Curve (b) in Figure 4 shows a baseline subtracted cyclic voltammogram of RuTPP-SWCNTs-Si, which is similar to the electrochemical behavior of the $RuTPP(CO)(C_6H_5N)$ complex in CH_2Cl_2 solution on a gold electrode (shown as an inset in Figure 4). It is clear that there are a pair of redox peaks at 742 and 1096 mV with very similar peak intensities which is completely consistent with the DPV results. The fwhm is 130 mV which is greater than the theoretical value for a single bound species implying that there are a variety of interaction environments for the attached ruthenium porphyrin molecules on the carbon nanotubes.

(56) Liu, Z. F.; Shen, Z. Y.; Zhu, T.; Hou, S. F.; Ying, L. Z.; Shi, Z. J.; Gu, Z. N. *Langmuir* **2000**, *16*, 3569–3573.
(57) Gooding, J. J. *Electrochim. Acta* **2005**, *50*, 3049–3060.

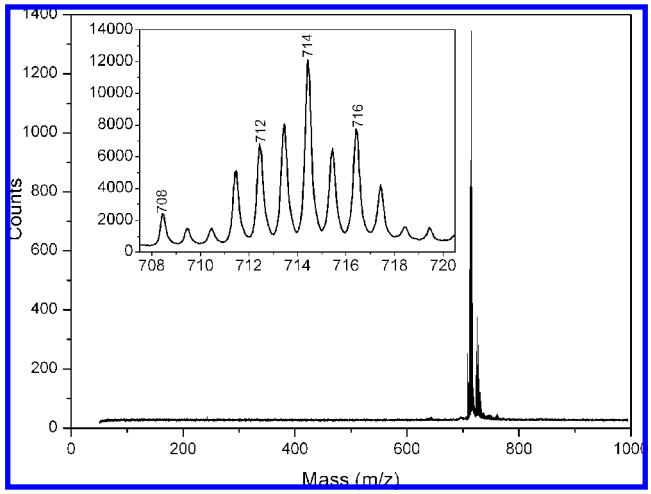

Figure 6. LDI-TOF-MS of desorbed and ionized RuTPP(CO) from the surface.

Table 1. *M*/*z* Peaks and Their Observed and Theoretical Relative Intensities

m/*z* peak (amu)	observed relative intensity (%)	theoretical relative intensity (%)
708	13.8	13.4
709	8.9	6.6
710	8.6	6.1
711	40.9	33.1
712	51.9	45.9
713	64.1	59.7
714	100	100
715	50.4	42.7
716	60.7	54.2
717	26.1	23.2
718	8.3	5.3

The electrochemical oxidation/reduction of ruthenium porphyrins has been reported in nonaqueous media such as CH_2Cl_2,[58] THF,[59] CH_3CN,[60] and so on. (TPP)Ru(CO)(py) can be oxidized in CH_2Cl_2 by two successive one-electron oxidations which occur on a platinum electrode at 0.81 V and potential greater than 1.1 V vs SCE.[61,62] The peak positions observed on ruthenium porphyrin coordinated to the SWCNTs-Si surface via 4-aminopyridine are very close to those positions. The first oxidation corresponds to the formation of $[(TPP)Ru^{II}(CO)(py)]^+$. The product of $[(TPP)Ru^{II}(CO)(py)]^+$ oxidation is assigned as an abstraction from the metal center at the second oxidation.[63,64] The surface concentration of ruthenium porphyrin molecules can be determined using the areas under the oxidation peaks of the voltammograms.[65] These measurements indicate that there are 3.44×10^{-8} mol cm^{-2} ruthenium porphyrin molecules,

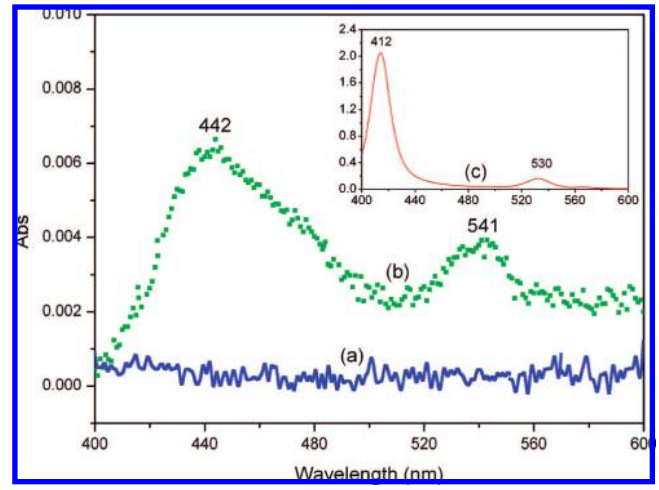

Figure 7. Solid-state UV−vis spectra of (a) SWCNTs-Si surface, (b) RuTPP-SWCNTs-Si surface, and (c) RuTPP(CO)EtOH in DMF.

which is about 250 times greater than zinc(II) trimesitylporphyrin directly attached to Si(100) surfaces[33,66] and about 3 times less than surface mounted ferrocenemethanol onto SWCNT arrays directly anchored to silicon(100).[19] This lower concentration is likely due to the two-step process used to attach the porphyrin to the nanotubes in contrast to the one-step process used to attach the ferrocenemethanol as well as the larger size of the porphyrin molecule which may prevent reaction at some sites. Obviously, due to the two readily available oxidization states, the ruthenium porphyrin coordinated SWCNTs-Si nanostructure could serve as the active storage medium in molecular memory devices with information stored in the discrete redox states of the molecules.

Atomic Force Microscopy (AFM) and Laser-Desorption Time-of-Flight Mass Spectrometry (LDI-TOF-MS). Figure 5a shows the tapping mode AFM image for the RuTPP-SWCNTs-Si surface with the protrusions characteristic of vertically oriented nanotubes. There is a distribution of nanotube heights observed ranging up to 120 nm with a broad peak in the distribution centered at about 24 nm. The width of the nanotube bundles varies from 10 to 400 nm with maximum distribution at about 75 nm. The image of the RuTPP-SWCNTs-Si surface is completely consistent with our previous imaging of similar surfaces.[19] Successful coordination of the ruthenium porphyrin onto the surface was confirmed in a novel fashion by LDI-TOF-MS analysis. Laser desorption is a relatively soft ionization method for the analysis of single molecules and mixtures.[67] Laser light at 337 nm was provided by the N_2 laser of the spectrometer providing excitation energy to the surface. At this wavelength both the SWCNT and RuTPP moieties of the surface efficiently absorb light. Thus the absorption of light by the surface results in concomitant desorption and ionization of the ruthenium porphyrin moiety. The LDI-MS analysis of the surface proceeds through initial breaking of the coordination bond of the supramolecular complex, leading to the detection of the ruthenium porphyrin as depicted in the LDI-MS spectrum in Figure 6. The metalloporphyrin derivative bereft of the axial carbonyl ligand was the major species detected in the mass spectrum, possessing a molecular ion at $m/z = 714$ amu. Table

(58) Stulz, E.; Sanders, J. K. M.; Montalti, M.; Prodi, L.; Zaccheroni, N.; De Biani, F. F.; Grigiotti, E.; Zanello, P. *Inorg. Chem.* **2002**, *41*, 5269–5275.
(59) Mu, X. H.; Kadish, K. M. *Langmuir* **1990**, *6*, 51–56.
(60) Brown, G. M.; Hopf, F. R.; Ferguson, J. A.; Whitten, D. G.; Meyer, T. J. *J. Am. Chem. Soc.* **1973**, *95*, 5939–5942.
(61) Malinski, T.; Chang, D.; Bottomley, L. A.; Kadish, K. M. *Inorg. Chem.* **1982**, *21*, 4248–4253.
(62) Kadish, K. M.; Hu, Y.; Tagliatesta, P.; Boschi, T. *J. Chem. Soc., Dalton Trans.* **1993**, 1167–1172.
(63) Kadish, K. M.; Leggett, D. J.; Chang, D. *Inorg. Chem.* **1982**, *21*, 3618–3622.
(64) Kadish, K. M.; Chang, D. *Inorg. Chem.* **1982**, *21*, 3614–3618.
(65) Laviron, E. *J. Electroanal. Chem.* **1979**, *101*, 19.
(66) Li, Q. L.; Mathur, G.; Gowda, S.; Surthi, S.; Zhao, Q.; Yu, L. H.; Lindsey, J. S.; Bocian, D. F.; Misra, V. *Adv. Mater.* **2004**, *16*, 133–137.
(67) Schalley C. A., Ed. *Analytical Methods in Supramolecular Chemistry*; Wiley-VCH Verlag GMbH & Co: Weinheim, Germany, 2007.

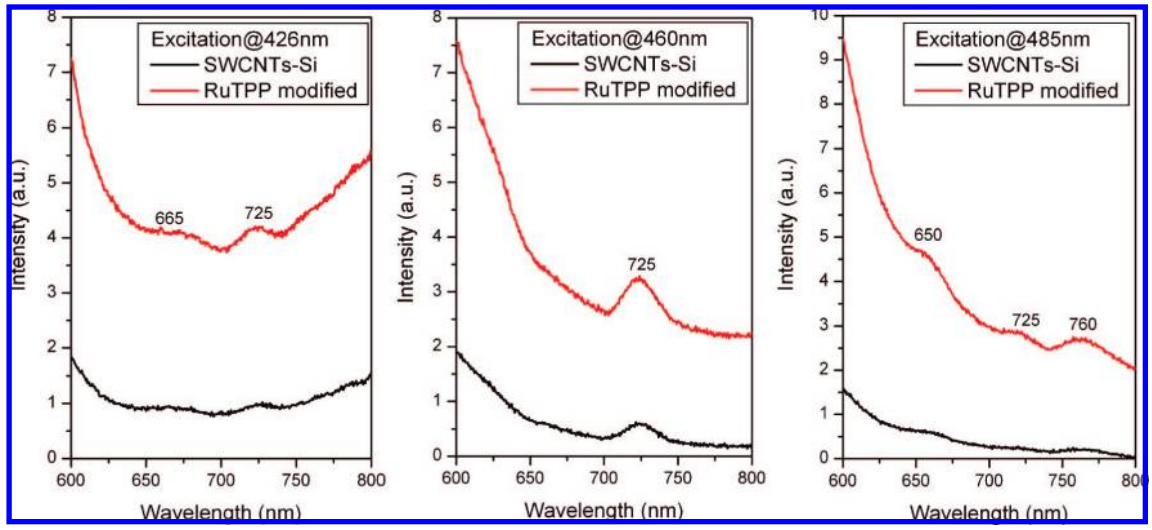

Figure 8. Fluorescence emission spectra of SWCNTs-Si surfaces and ruthenium porphyrin modified SWCNTs-Si surfaces excited by different wavelengths, where ruthenium porphyrin modified SWCNTs-Si surfaces were obtained by incubating SWCNTs-Si surfaces in 4-aminopyridine/DMF solution and then in ruthenium porphyrin/chloroform solution for 24 h, respectively.

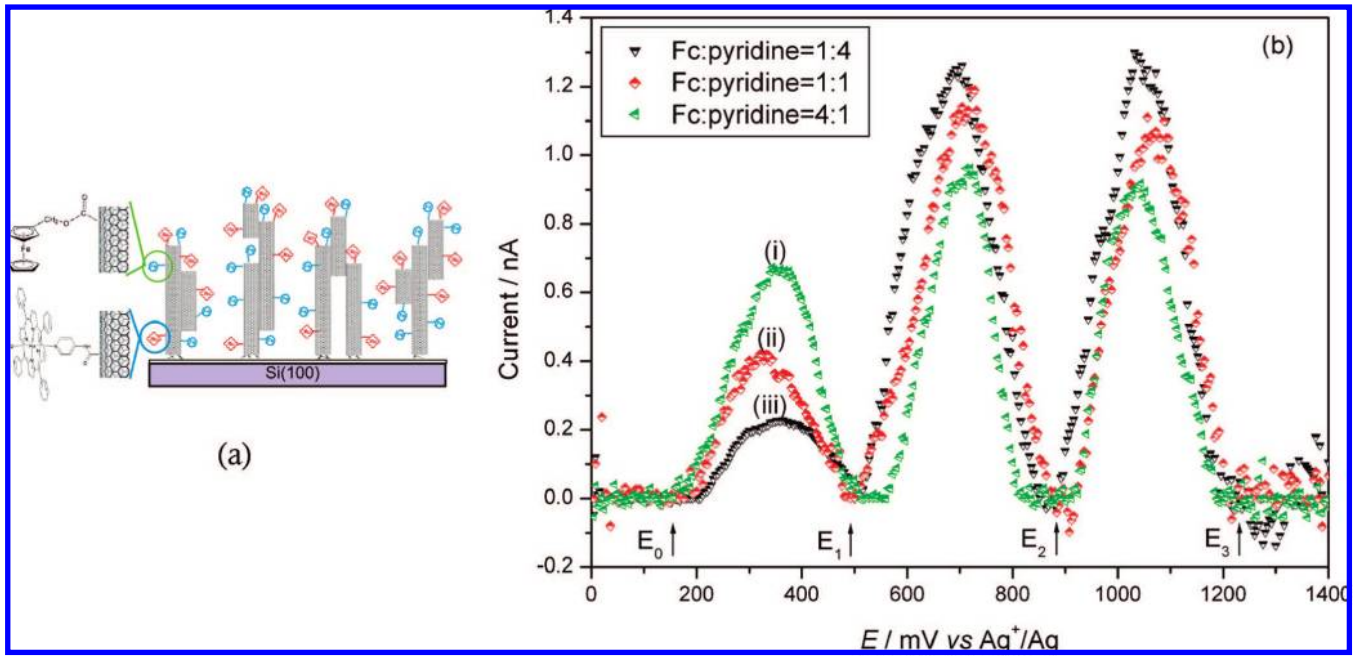

Figure 9. (a) Schematic representation of mixed assembly of ferrocenemethanol/ruthenium porphyrin onto carbon nanotube arrays. (b) Differential pulse voltammograms of mixed assembly of ferrocene/porphyrin onto carbon nanotube arrays in 0.1 mol L^{-1} $TBAPF_6/CH_2Cl_2$ solution at the scan rate 20 mV s^{-1} by immersing in mixtures with different molar ratios of ferrocenemethanol and 4-aminopyridine, and then incubating in ruthenium porphyrin/CH_2Cl_2 solution.

Table 2. Surface Concentration of Ferrocene and Ruthenium Porphyrin Immobilized onto Single-Walled Carbon Nanotube Arrays

ratio of ferrocene and pyridine	surface concn of ferrocene [mol cm^{-2}]	surface concn of porphyrin [mol cm^{-2}]
1:0[19]	9.26×10^{-8}	-
4:1	1.65×10^{-8}	1.83×10^{-8}
1:1	1.01×10^{-8}	2.72×10^{-8}
1:4	6.18×10^{-9}	3.13×10^{-8}
0:1	-	3.44×10^{-8}

1 lists the *m*/*z* peaks and their observed and theoretical relative intensities, where the theoretical relative intensities of ruthenium porphyrin are obtained by the software ChemDraw Pro V11.0. From Table 1, the observed relative peak intensities of the LDI-TOF-MS spectrum are in good agreement with their theoretical relative intensities.

UV−visible Spectroscopy. Figure 7 shows the UV−visible spectra of the SWCNTs-Si and RuTPP-SWCNTs-Si surfaces. Comparison of the two spectra shows that, upon incorporation of the macrocyclic chromophore onto the surface, the UV−vis properties of the surface are enhanced. The precursor surface exhibits no significant absorbance properties in the visible region. In contrast, the spectrum of the RuTPP-SWCNTs-Si surface exhibits strong, broad absorptions centered at 440 and 541 nm. The absorptions of the porphyrin functionalized surface are consistent with the position and molar absorptivity of the

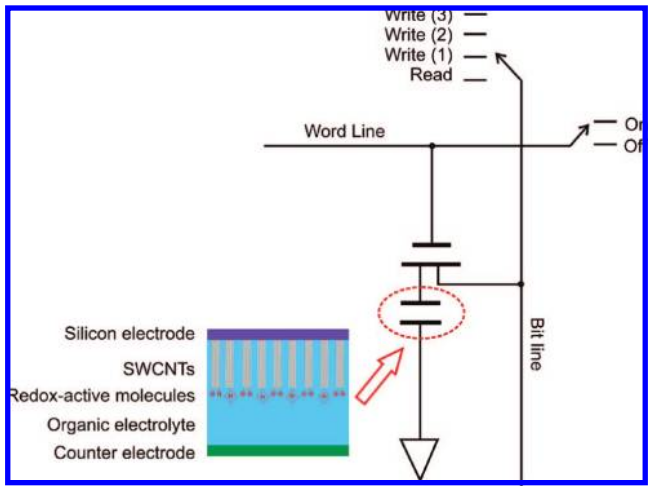

Figure 10. Schematic representation of multibit molecular storage element using mixed assembly of ferrocene/porphyrin onto carbon nanotube arrays as information storage medium.

Soret and Q-band absorptions of the metalloporphyrin in solution, featured as an inset in Figure 7.

Steady-State Fluorescence Spectroscopy. Figure 8 shows the emission spectra from SWCNTs-Si and RuTPP-SWCNTs-Si as obtained by steady-state fluorescence spectroscopy. Initial fluorescence experiments were conducted on RuTPP-SWCNTs-Si surfaces obtained from immersion of the 4-aminopyridine functionalized SWCNTs-Si surface in RuTPP(EtOH)CO for 24 h. The emission behavior of the SWCNTs-Si surface was investigated by irradiating the surface at 426, 460, and 485 nm. Irradiation of the surface at 426 nm afforded maxima possessing a weak emission intensity at 665 and 725 nm. By moving the excitation wavelength to 460 nm, the surface produced an emission maximum at 725 nm with a greater intensity than when excited at 426 nm, and irradiation of the SWCNTs-Si surface at 485 nm produced weak emissions at 650, 725, and 760 nm. Irradiation of the RuTPP-SWCNTs-Si surface at 426, 460, and 485 nm was performed in a similar manner to that of the precursor surface, but no new maxima were observed upon recording the emission spectrum. The wavelengths chosen all coincide with the enhanced absorption of the chromophore on the RuTPP-SWCNTs-Si surface. The outcome was a noticeable enhancement in the emission intensity of all the maxima derived from the SWCNTs-Si component of the surface. Thus the lack of porphyrin-derived emission coupled with the enhancement of SWCNTs-Si emission intensity on the porphyrin functionalized surface was ascribed to a photoinduced energy transfer occurring on the surface. Furthermore, it is envisaged that the energy transfer is occurring from the porphyrin to the SWCNT, then possibly to the Si on the surface.

Mixed Assembly of Ferrocene/Porphyrin onto Carbon Nanotube Arrays. Mixed assembly of ferrocene/porphyrin onto carbon nanotube arrays was prepared by incubating SWCNTs-Si in mixtures of 4-aminopyridine and ferrocenemethanol in DMF solvent and then in a ruthenium porphyrin/CH_2Cl_2 solution. Figure 9 a shows the schematic representation of the mixed assembly of ferrocenemethanol/ruthenium porphyrin onto carbon nanotube arrays and their differential pulse voltammograms. It is clear that each curve shows three well separated peaks at around 370, 720, and 1048 mV. Moreover when increasing the molar ratio of Fc/pyridine in DMF solutions, the peak current at 370 mV becomes bigger, but the peak currents at both 720 and 1048 mV get smaller. Obviously the peak at 370 mV is attributed to the oxidation of surface-mounted ferrocenemethanol molecules as observed previously.[19] The peaks at both 720 and 1048 mV originate from the oxidation of ruthenium porphyrin. Compared to the voltammetric behavior of Fc-SWCNTs-Si and RuTPP-SWCNTs-Si, mixed assembly of ferrocene/porphyrin onto carbon nanotube arrays exhibits one neutral and three oxidation states, which can represent 2 bit information.

Table 2 lists the surface concentration of ferrocene and ruthenium porphyrin on carbon nanotube arrays as determined by DPV peak areas combined with the geometric area of the sample used in the experiment. The surface concentration of ferrocenemethanol for pure Fc-SWCNTs-Si is higher than that of ruthenium porphyrin for RuTPP-SWCNTs-Si. The higher coverage is mainly attributed to the smaller size of ferrocenemethanol compared to ruthenium porphyrin. However at the molar ratio of 1:1, the surface concentration of ferrocenemethanol is lower than that of ruthenium porphyrin. This result indicates that the ferrocenemethanol molecules have a slower attachment rate to the carboxylic groups of SWCNTs compared to 4-aminopyridine in DMF.[68] As the molar ratio of ferrocenemethanol and 4-aminopyridine in solution decreases from 4:1 to 1:4, the molar ratio of surface concentration of ferrocenemethanol and ruthenium porphyrin decreases from 0.90 to 0.20. Obviously altering the ratio of the two redox-active species in the deposition solution allows tuning the coverage of different molecules in the mixed assembly.

Figure 10 shows the schematic representation of a multibit molecular storage element based on the mixed assembly of ferrocene/porphyrin onto carbon nanotube arrays as an information storage medium. The multibit molecular storage elements can be arranged in a matrix, and each molecular storage element can be accessed by an electrical address. Compared to the current dynamic random access memory (DRAM), the capacitor in a basic DRAM cell is replaced by an electrochemical cell. In order to write information to the molecular storage cell, a write voltage (E_w) is applied to the bitline and the wordline is set to high to open the field effect transistor (FET). If the E_w is lower than E_0 (marked in Figure 9b), the immobilized ferrocene and porphyrin molecules stay at their neutral states, and hence, a logic state "00" is written to the cell; if the E_w is set to E_1 (marked in Figure 9b), the immobilized ferrocene molecules turn to their oxidation state, and thus a logic state "01" is written to the cell; if the E_w is set to E_2, the immobilized porphyrin molecules convert to their first oxidation state, so a logic state "10" is written to the cell; if the E_w is higher than E_3, the immobilized porphyrin molecules switch to their second oxidation state, and therefore a logic state "11" is written to the cell. The applied potential is then disconnected, and the electrochemical cell stores the information (actually an oxidation state of storage molecules) for a period of time. When the time comes to access the stored information, the wordline goes high to open the FET. The open circuit potential (E_{ocp}) of the electrochemical cell, which is determined by the stored oxidation state, is sensed using an amplifier at the end of the bitline. If the E_{ocp} is less than E_0, it means "00". If $E_0 < E_{ocp} < E_1$, information is "01"; if $E_1 < E_{ocp} < E_2$, information is "10"; if $E_2 < E_{ocp} < E_3$, it denotes "11".

(68) Flavel, B. S.; Yu, J.; Shapter, J. G.; Quinton, J. S. *Carbon* **2007**, *45*, 2551–2558.

Conclusions

Ruthenium porphyrin functionalized single-walled carbon nanotube arrays have been prepared using coordination of the axial position of the metal ion onto 4-aminopyridine preassembled single-walled carbon nanotubes directly anchored to a silicon(100) surface (SWCNTs-Si). Electrochemical results show two successive one-electron reversible redox waves and that the surface concentration of ruthenium porphyrin molecules is 3.44×10^{-8} mol cm^{-2}. Optical properties indicate that the immobilization of ruthenium porphyrin enhances the light absorption of SWCNTs-Si surfaces in the visible light region. Moreover mixed assembly of ferrocene/porphyrin onto carbon nanotube arrays has been achieved by altering the ratio of two redox-active species in the deposition solution. These results suggest that these ruthenium porphyrin modified electrodes are excellent candidates for molecular memory devices and light harvesting antennae.

Acknowledgment. The authors would like to thank Ms. Rachel Lowe and Ms. Georgia Guild for their help on the measurement of Laser-Desorption Time-of-Flight Mass Spectrometry (LDI-TOF-MS).

Supporting Information Available: The preparation and characterization of the porphyrin RuTPP(CO)EtOH used in this study are reported. This material is available free of charge via the Internet at http://pubs.acs.org.

JA801142K